Development of a well impairment model for predicting geothermal clogging (DIMOPREC)

Hussain, A.A.A.; Meulenbroek, B.J.; Wolf, K.H.A.A.; Khoshnevis Gargar, N.; Bruining, Hans; van der Star, Wouter; Claringbould, Han; Llaneza, Isabelle

Publication date
2022

Document Version
Final published version

Citation (APA)
Hussain, A. A. A., Meulenbroek, B. J., Wolf, K. H. A. A., Khoshnevis Gargar, N., Bruining, H., van der Star, W., Claringbould, H., & Llaneza, I. (2022). *Development of a well impairment model for predicting geothermal clogging (DIMOPREC)*. Advance online publication.

Important note
To cite this publication, please use the final published version (if applicable).
Please check the document version above.

Development of a well impairment model for predicting geothermal clogging (DIMOPREC)

PI/project leader: Ahmed Hussain (TU Delft)
Project members: Bernard Meulenbroek (TU Delft),
Wouter van der Star (Deltares), Han Claringbould (Veegeo),
Aayla Reerink (previously at Veegeo),
Negar Khoshnevis Gargar (previously at Deltares and TU Delft),
Hans Bruining (previously at TU Delft)
Coordinator: Karl-Heinz Wolf (TU Delft)

Abstract

When producing heat from a geothermal well, the produced water cools down in the heat exchanger, and experiences a lower pressure in the surface processing-facility (1 – 10 bar) than in the reservoir (100 – 300 bar). The decrease in pressure may cause CO_2 to come out of solution, resulting in a higher pH. This decrease in temperature and increase in pH of the processed water-may cause mineralization or some minerals to dissolve in the near-well-bore area when reinjected. After the produced water is cooled down, it is reinjected into the reservoir through an injection well. Mineral precipitation in the reservoir restricts the flow path of the injected water, resulting in reduced injectivity. Consequently, more energy is required by the injection pump, which results in additional costs, and thereby reduces the project's economic return.

When numerically modeling mineralization in a geothermal reservoir, accounting for the reaction kinetics can be computationally expensive. The simulations can be made less expensive by assuming local equilibrium between the reactants and reaction-products; but using this approach might give results that are not in agreement with experimental findings.

Here we present an analytical model for mineral precipitation in a low-enthalpy geothermal reservoir. We compare the kinetics of the relevant reaction terms with respect to the transport terms (heat and flow) to determine whether the local equilibrium approach (LEA) or kinetics approach (KA) is appropriate for modeling a specific reaction. We focus on the near-wellbore region in the reservoir, where precipitation can behave as a 'skin'; when assuming radial-flow, precipitation in the near-wellbore region has a more dramatic impact on the injectivity than precipitation further downstream in the reservoir.

Using numerical simulations we validate the approach to use different methods of geochemical modelling based on the reaction speed and its potential impact on computation time.

Based on our analysis on mineralization in the near-wellbore-region, the three different reaction regimes can be distinguished when comparing the time-scale of reaction to the time-scale of transport, viz.: (1) fast reactions (mineralization can be considered instantaneous and modelling these reactions using LEA or KA does not lead to significantly different simulation results); (2) very slow reactions (no significant change in ion concentrations in the region of interest, whether these reactions are modelled using LEA or KA); (3) reaction/transport intermediate zone (using LEA leads to significantly different simulation results compared to KA).

Accounting for these classifications allows simplification of the current numerical geochemical-models, while still accounting for relevant kinetics of mineralization. This approach was tested using a numerical model of mineralization in a geothermal reservoir.

We developed a SKID which allows to measure various properties of the produced water at different points in the process facility. The information retrieved from the SKID can be used to model mineral precipitation in the surface facility and in the reservoir.

Furthermore, two *spin-off* research studies were conducted: 1) lithium in geothermal water and 2) radioactive lead precipitation in geothermal facilities.

One of the valuable metals dissolved in geothermal water is lithium. We find that multiple locations in the Netherlands where lithium concentration in aquifers can be higher 25 ppm: Californie (22-38 ppm) and Akkrum-13 (47 ppm). These locations are in the vicinity (less than 50 km) of igneous depositions. Moreover, in our sample-set we find a correlation between the lithium concentration and rubidium concentration (N=13 for samples with both measured).

Concerning radioactive lead precipitation we investigate a field-case study where galena precipitate is filtered in the surface facility. We model this geothermal system in PHREEQC. The PHREEQC model shows that a majority of the collected galena is likely produced in solid phase from the reservoir, and a smaller fraction is formed within the geothermal facility.

1 Introduction

In low-enthalpy geothermal projects warmer water (temperature between 60 - 100°C) is produced from an underground reservoir, which can be several kilometers below the surface. As water flows from the bottom of the production-well towards the surface-facilities, it experiences a significant decrease in pressure (typically 100 – 200 bar), which may lead to CO_2 gas to come out of solution, resulting in a pH increase. Within the surface-facilities the water will experience a significant decrease in temperature at the heat-exchanger. This increase in pH and decrease in temperature may result in mineralization and dissolution [1]. For example montmorillonite and chalcedony may precipitate [2], and some rock minerals, such as carbonates, may dissolve into the injected water near the injection well [3]. As the relatively colder water flows downstream in the reservoir it will be heated by the reservoir rock. Some minerals are more soluble in water at lower temperature, such as carbonates, and thus the water may be undersaturated with carbonates near the inlet, and become supersaturated with these carbonates further downstream, due to the increase in temperature, and therefore they may precipitate. Conversely, some minerals have a higher solubility in water at a higher temperature, and therefore precipitation may occur near the inlet and dissolution may occur further downstream.
Modeling mineralization is relevant because mineralization may contribute to a gradual decrease in injectivity of sandstone geothermal reservoirs, such as in China [2]. However, [4] argues that when injecting colder water into reservoirs the main source of damage to wells and formations is due to fines invasion and migration, and not precipitation.
Mineralization in geothermal-reservoirs can be modelled using various methods, among which a Local Equilibrium Approach (LEA) and a Kinetic Approach (KA) are widely used [4–6]. Both these methods involve the maximum solubility of a mineral in a solution, given by the equilibrium constant, and the Ion Activity Product (IAP), which is approximately equal to the product of the concentration of the ions of a mineralization reaction. The equilibrium constant can be given as a function of temperature, such as in Equation 65 [7], or as a constant. If the IAP is larger than the equilibrium constant, the solution is 'supersaturated', if equal 'saturated', and if smaller 'undersaturated'.
When using a LEA to model a supersaturated solution, it is assumed mineralization occurs instantaneously and the solution is saturated. Similarly if a mineral in solid state is in contact with a solution, that is undersaturated with that mineral, the mineral will dissolve instantaneously until the solution is saturated.
Whereas when modelling mineralization with a KA the reaction rates are taken into account. To obtain the necessary information to model mineralization using a KA, usually an Arrhenius-type function is fit to the experimentally observed kinetics in a range of ion concentrations, temperature, and sometimes pH; see for example [8–10]. Modelling mineralization using a kinetic approach requires more calculations every timestep compared to a local equilibrium approach; it is numerically more expensive than using a LEA. Furthermore, fewer input parameters are required to model mineralization using a LEA compared to using a KA. Although significant effort has been made to collect data on mineralization kinetics ([5, 6, 11]), the precipitation and dissolution kinetics of many minerals have not been studied or published.
This report is organized as follows: in chapter 2 we derive the relevant equations to model the flow of dissolved ions in the near well bore region and the precipitation of minerals with which the water is super-saturated. In chapter 3 we present an analytical model to calculate the concentration of the different ions in a porous medium. Hereafter we describe our numerical model and use it to validate our analytical approach in chapter 4. We then use our numerical approach to model a field case.

2 Derivation of the model equations (part of task 2a)

We are interested in a geothermal reservoir of height H around the injection well with radius R_w; this means that we choose cylindrical coordinates to describe our domain of interest D_3

$$D_3 = \{(r, \theta, z) \mid r \geq r_w,\ 0 \leq \theta \leq 2\pi, 0 \leq z \leq H\ \}. \tag{1}$$

Furthermore we assume that our reservoir is homogeneous in the z-direction, which means that our problem becomes effectively a two-dimensional domain D_2

$$D_2 = \{(r, \theta) \mid r \geq r_w,\ 0 \leq \theta \leq 2\pi\ \}. \tag{2}$$

In our analytical approach we also assume homogeneity in the $\theta-$direction, which means that we have an effective domain $D_{1,a}$

$$D_{1,a} = \{(r \mid r \geq r_w\}. \tag{3}$$

In our numerical approach we look at two cases; a segment of D_2, viz. $D_{2,n}$

$$D_{2,n} = \{(r, \theta) \mid r_w \leq r \leq r_{end},\ \theta_1 \leq \theta \leq \theta_2\ \}. \tag{4}$$

The (numerical) upper bound $r = r_{end}$ has to be chosen large enough (i.e. the numerical results should be independent of this particular choice). We also look at an effectively one-dimensional numerical domain $D_{1,n}$

$$D_{1,n} = \{(r \mid r_w \leq r \leq r_{end}\} \tag{5}$$

which allows us to compare our numerical and analytical results.

2.1 Velocity field

We assume incompressible flow, which means the continuity equation for the Darcy-velocity $\mathbf{u}$ yields

$$\nabla \cdot \mathbf{u} = 0. \tag{6}$$

Furthermore we assume Darcy's law, which means that we have

$$\mathbf{u} = -\frac{k}{\mu}\nabla p, \tag{7}$$

where k is the (possibly spatially dependent) permeability, μ is the viscosity and p the pressure.

At the injection well, water is injected at a constant flux Q_{inj}, which means that we have constant radial velocity at the injection well

$$\mathbf{u} = \frac{Q_{inj}}{2\pi H r_w}\hat{\mathbf{r}} = u_{inj}\hat{\mathbf{r}} \text{ at } r = r_w, \tag{8}$$

where we denote the unit vector in the radial direction by $\hat{\mathbf{r}}$ and where we lumped a few constants together in $u_{inj} = \frac{Q_{inj}}{2\pi H r_w}$ for convenience.

2.2 Transport equation

The transport of the i^{th} species A_i is modelled using a convection-diffusion-reaction equation for its molal concentration C_i (mol/kgw)

$$\phi\frac{\partial C_i}{\partial t} + \nabla \cdot \mathbf{J}_i = -\phi S_i, \tag{9}$$

where the flux $\mathbf{J}_i$ is given by the sum of a convective and a diffusive part

$$\mathbf{J}_i = C_i\mathbf{u} - \phi D\nabla C_i, \tag{10}$$

where ϕ is the porosity and D the diffusion coefficient. The net precipitation rate S_i is the sum all contributions S_i^j of all N reactions in which A_i is involved, i.e.,

$$S_i = \sum_{j=1}^{N} S_i^j. \tag{11}$$

The terms S_i^j are given in terms of temperature T and concentrations of all species $C_i,\ i = 1,\ \ldots\ M$ that are included in the simulation. The terms S_i^j are modelled using the law of mass action, i.e., for a reaction of the form

$$aA + bB \leftrightarrow cC + dD, \tag{12}$$

the forward and backward rates R_+ and R_- are given by

$$R_+ = SAK_+ a_A^a a_B^b,\ R_- = SAK_- a_C^c a_D^d, \tag{13}$$

where a_A denotes the (dimensionless) activity of A, $K_\pm$ are rate constants [mol/m^2 s] and SA is the specific surface area [m^2]. The activity is related to the concentration via the (dimensionless) activity coefficient γ_A as follows

$$a_A = \frac{\gamma_A C_A}{\gamma_r C_r}, \tag{14}$$

where C_r is a (hypothetical) 1 molal reference solution and γ_r its actitvity coefficient, which is also set to one. The activity coefficient γ_A is given in terms of temperature, e.g., by the Debye-Hückel relation. We are mainly interested in precipitation/dissolutionreactions of the form

$$A_i B_{ij} \leftrightarrow A_i + B_{ij}. \tag{15}$$

This leads to a precipitation R_{prec} (backward) rate of

$$R_{prec} = SA_{prec}^j K_{prec}^j a_{A_i} a_{B_{ij}} = SA_{prec}^j K_{prec}^j IAP^j, \tag{16}$$

because in this case the ionic activity product IAP^j equals the product of the activities of A_i and B_{ij}. The dissolution (forward) rate R_{diss} is given by

$$R_{diss} = SA_{diss}^j K_{diss}^j a_{A_i B_{ij}} = SA_{diss}^j K_{diss}^j, \tag{17}$$

because the activity of a solid is assumed one. This yields a net precipitation rate S_i^j

$$S_i^j = R_{prec} - R_{diss} = SA_{prec}^j K_{prec}^j IAP^j - SA_{diss}^j K_{diss}^j =$$

$$SA_{diss}^j K_{diss}^j \left(\frac{SA_{prec} K_{prec}^j IAP^j}{SA_{diss} K_{diss}^j} - 1 \right) = SA_{diss}^j K_{diss}^j \left(\frac{IAP^j}{K_{eq}^j} - 1 \right), \tag{18}$$

where we used the equilibrium constant

$$K_{eq}^j = \frac{SA_{diss} K_{diss}^j}{SA_{prec} K_{prec}^j}. \tag{19}$$

Note the equilibrium constant equals the solubility product, because at equilibrium we have

$$R_{diss} = R_{prec} \Rightarrow SA_{diss}^j K_{diss}^j = SA_{prec}^j K_{prec}^j a_{A_i} a_{B_{ij}} \Rightarrow K_{eq}^j = \frac{SA_{diss} K_{diss}^j}{SA_{prec} K_{prec}^j} = a_{A_i} a_{B_{ij}}. \tag{20}$$

For more general reactions, the following expression $\tilde{S}_i^j$ can be used for the net precipitation rate

$$\tilde{S}_i^j = \nu_i^j SA_{diss}^j K_{diss}^j \left(\left[\frac{IAP^j}{K_{eq}^j} \right]^{\theta_0} - 1 \right)^{\eta_0}, \tag{21}$$

where ν_i^j is the stoichiometric coefficient and θ_0 and η_0 are fitting parameters.

We will now discuss how the rate constants are modelled in terms of temperature. The dissolution reaction constant K_{diss}^j is modelled as function of temperature T using an Arrhenius type equation

$$K_{diss}^j = A^j e^{-\frac{E_a^j}{RT}}, \tag{22}$$

where A^j is the Arrhenius pre-exponential factor [mol/(m^2 s)], E_a is the Arrhenius activation energy [J/mol], R is the universal gas constant [J/(mol K)] and T is temperature [K]. The equilibrium constant K^j_{eq} is modelled using the phenomenological relation

$$\log_{10} K^j_{eq} = A_1 + A_2 T + \frac{A_3}{T} + A_4 \log_{10} T + \frac{A_5}{T^2} + A_6 T^2, \tag{23}$$

where the coefficients $A_1, \ldots, A_6$ are determined experimentally.

The precipitation rate is not always available in literature, in these cases we can use the dissolution rate K^j_{diss} to obtain the precipitation rate as follows [5, 12].

$$K^j_{eq} = \frac{K^j_{diss}}{K^j_{prec}}. \tag{24}$$

2.2.1 Summary transport equation

For each of the M species we have a reaction-diffusion-convection equation

$$\phi \frac{\partial C_i}{\partial t} + \nabla \cdot (C_i \mathbf{u}) - \nabla \cdot (\phi D \nabla C_i) = -\phi S_i, \tag{25}$$

where the net precipitation rate S_i is given in terms of the temperature and the concentrations C_i as follows

$$S_i = \sum_{j=1}^{N} \nu^j_i S A^j K^j_{diss} \left(\left[\frac{IAP^j}{K^j_{eq}} \right]^{\theta_0} - 1 \right)^{\eta_0}, \tag{26}$$

where IAP^j are the ionic activity products (depending on the concentrations); the parameters K^j_{diss} and K^j_{eq} dependend on the temperature:

$$K^j_{diss} = A^j e^{-\frac{E^j_a}{RT}}, \ \log_{10} K^j_{eq} = A_1 + A_2 T + \frac{A_3}{T} + A_4 \log_{10} T + \frac{A_5}{T^2} + A_6 T^2. \tag{27}$$

2.3 Initial and boundary conditions

For the pressure we have a second order equation in the spatial variables, which means that a boundary condition on all four boundaries (for $D_{2,n}$) or for both boundaries (for $D_{1,n}$ and $D_{1,a}$) is required. For the concentrations we have second order equation in the spatial variables and a first order equation in time, which means that both an initial condition has to be specified and boundary conditions on all (4 resp. 2) boundaries.

2.3.1 Boundary conditions for the pressure

At the inlet we have constant inflow (8)

$$\mathbf{u} = u_{inj} \hat{\mathbf{r}} \text{ at } r = r_w, \tag{28}$$

which means that we the following Neumann condition for the pressure

$$\frac{\partial p}{\partial r} = -\frac{\mu}{k} \cdot u_{inj} \text{ at } r = r_w. \tag{29}$$

Water travels a finite distance in finite time, which means that the influence of the injection well is negligible far away

$$\frac{\partial p}{\partial r} \to 0 \text{ as } r \to \infty. \tag{30}$$

Finally (for the $D_{2,n}$ case) we assume that the lateral boundaries are impermeable, i.e.,

$$\frac{\partial p}{\partial \theta} = 0 \text{ for } \theta = \theta_1 \text{ and } \frac{\partial p}{\partial \theta} = 0 \text{ for } \theta = \theta_2. \tag{31}$$

2.3.2 Initial and boundary conditions for the concentration

Initially all concentrations are constant and at equilibirum

$$C_i(r,0) = C_{i,0} \text{ (constant)}. \tag{32}$$

At the inlet, we have a Danckwert's condition; the concentration flux just before the inlet equals the concentration flux just after the inlet:

$$\mathbf{J}_i(r_w^-,t) = \mathbf{J}_i(r_w^+,t), \tag{33}$$

where the flux is given in equation (10). The velocity at the inlet is continuous and given in equation (8), which means that we find

$$C_i(r_w^-,t)u_{inj} - \phi D\frac{\partial C}{\partial r}(r_w^-,t) = C_i(r_w^+,t)u_{inj} - \phi D\frac{\partial C}{\partial r}(r_w^+,t). \tag{34}$$

For $r = r_w^-$ we are inside the injection well, which means that we have the (constant) injection concentration C_i^{inj}

$$C_i(r_w^-,t) = C_i^{inj} \text{ (constant)}, \ \frac{\partial C}{\partial r}(r_w^-,t) = 0 \tag{35}$$

This yields a Robin boundary condition for the concentration

$$C_i(r_w^+,t)u_{inj} - \phi D\frac{\partial C}{\partial r}(r_w^+,t) = C_i^{inj}u_{inj}. \tag{36}$$

For most cases, however, the diffusion is much smaller than the convection and this boundary condition effectively behaves as a Dirichlett boundary condition

$$C_i(r_w^+,t) = C_i^{inj}. \tag{37}$$

The other boundary conditions for the concentration profiles are similar to the conditions of the pressure profile (due to the same reasoning), i.e.,

$$\frac{\partial C_i}{\partial r} \to 0 \text{ as } r \to \infty \tag{38}$$

and

$$\frac{\partial C_i}{\partial \theta} = 0 \text{ for } \theta = \theta_1 \text{ and } \frac{\partial C_i}{\partial \theta} = 0 \text{ for } \theta = \theta_2. \tag{39}$$

3 Analytical approach (task 2a)

In [13] a simplified version of the problem was analyzed and solved.

3.1 Velocity field

In our analytical approach, we assume a homogeneous reservoir, which means that we only have r and t (time) as independent variables (i.e. no dependence on θ). Furthermore we have, due to our injection condition (8) that flow is purely in the r-direction, which means that we have

$$\mathbf{u} = u(r)\hat{\mathbf{r}}. \tag{40}$$

Using the continuity equation (6) we can derive an explicit expression for $u(r)$ as follows

$$\frac{\partial}{\partial r}\left(ru(r)\right) = 0 \Rightarrow u(r) = \frac{C(t)}{r} \tag{41}$$

and using the boundary condition (8) we find an expression for $C(t)$

$$C(t) = \frac{Q_{inj}}{2\pi H} \text{ (constant)}, \tag{42}$$

which means that we have

$$u(r) = \frac{Q_{inj}}{2\pi H r} \tag{43}$$

3.2 Transport equation

The transport equation in domain $D_{1,an}$ in cylindrical coordinates simplifies (using equation (43))

$$\phi\frac{\partial C_i}{\partial t} + \frac{Q_{inj}}{2\pi Hr}\frac{\partial C_i}{\partial r} - D\phi\frac{1}{r}\frac{\partial}{\partial r}\left(r\frac{\partial C_i}{\partial r}\right) = -\phi S_i. \tag{44}$$

Furthermore, we make the following assumptions in order to simplify the reaction term:

1. Only two species A and B are involved and only one reaction of the form

$$AB \leftrightarrow A + B$$

.

2. The concentration of B is constant and much larger than the concentration of A, i.e.,

$$C_B \gg C_A \text{ and } C_B(r_w, t) = C_B(r, 0) \text{ (constant)} \Rightarrow C_B(r, t) = C_B(r, 0) \text{ (constant)}.$$

3. The parameters θ_0 and η_0 are one; note furthermore that the stoichiometric coefficient ν_i equals one too.

4. The activity coefficients are assumed to be one, which means that we have $a_A = \frac{C_A}{C_r} = \frac{C}{C_r}$, defining $C = C_A$. Similary we have $a_B = \frac{C_B}{C_r}$, which is constant due to assumption 2.

Using these assumptions, our reaction term (26) reduces to

$$S_i = SA \cdot K_{diss}\left(\frac{IAP}{K_{eq}} - 1\right), \tag{45}$$

where the ionic activity product is given by

$$IAP = \frac{C \cdot C_B}{C_R^2}. \tag{46}$$

Furthermore we only need to solve equation (44) for the concentration of species A, i.e., we need to solve

$$\phi\frac{\partial C}{\partial t} + \frac{Q_{inj}}{2\pi Hr}\frac{\partial C}{\partial r} - D\phi\frac{1}{r}\frac{\partial}{\partial r}\left(r\frac{\partial C}{\partial r}\right) = -\phi \cdot SA \cdot K_{diss}\left(\frac{C \cdot C_B}{C_R^2 K_{eq}} - 1\right). \tag{47}$$

Note that initially the reservoir is in equilibrium, so the reaction term equals zero if $C = C_0$; this allows us to simplify the RHS, because we have

$$\frac{C_0 \cdot C_B}{C_R^2 K_{eq}} - 1 = 0 \Rightarrow \frac{C_R^2 K_{eq}}{C_B} = C_0 \tag{48}$$

and we can rewrite equation (47)

$$\phi\frac{\partial C}{\partial t} + \frac{Q_{inj}}{2\pi Hr}\frac{\partial C}{\partial r} - D\phi\frac{1}{r}\frac{\partial}{\partial r}\left(r\frac{\partial C}{\partial r}\right) = -\phi \cdot SA \cdot K_{diss}\left(\frac{C}{C_0} - 1\right). \tag{49}$$

3.3 Scales and dimensionless variables

We are mainly interested in the flow around the injection well, so we choose as our characteristic scale r_c the well radius r_w, which leads to the dimensionless radial coordinate r_d

$$r_c = r_w \Rightarrow r_d = \frac{r}{r_c} = \frac{r}{r_w}. \tag{50}$$

As characteristic velocity v_c we choose the interstitial velocity at the characteristic distance, i.e.,

$$v_c = v(r_c) = \frac{Q_{inj}}{2\pi Hr_c\phi} \tag{51}$$

(note the inclusion of the porosity). From the characteristic velocity we obtain the characteristic time t_c and the dimensionless time t_d as follows

$$t_c = \frac{r_c}{v_c} = \frac{2\pi r_c^2 H\phi}{Q_{inj}},\ t_d = \frac{t}{t_c}. \tag{52}$$

As characteristic concentration C_c we choose the initial concentration C_0, the dimensionless concentration C_d is translated, such that $C_d = 0$ corresponds to equilibrium, as follows

$$C_d = \frac{C - C_0}{C_0}. \tag{53}$$

Using equations (50)-(53) we rewrite equation (49) in dimensionless form as follows

$$\phi\frac{C_0}{t_c}\frac{\partial C_d}{\partial t_d} + \frac{Q_{inj}}{2\pi H r_c r_d}\cdot\frac{C_0}{r_c}\frac{\partial C_d}{\partial r_d} - D\phi\frac{1}{r_c^2}\frac{1}{r_d}\frac{\partial}{\partial r_d}\left(r_d\frac{\partial C_d}{\partial r_d}\right) = -\phi\cdot SA\cdot K_{diss}C_d, \tag{54}$$

i.e.,

$$\frac{\partial C_d}{\partial t_d} + \frac{Q_{inj}t_c}{2\pi H r_c^2\phi}\cdot\frac{1}{r_d}\frac{\partial C_d}{\partial r_d} - \frac{Dt_c}{r_c^2}\frac{1}{r_d}\frac{\partial}{\partial r_d}\left(r_d\frac{\partial C_d}{\partial r_d}\right) = -\frac{SA\cdot K_{diss}\cdot t_c}{C_0}C_d, \tag{55}$$

which yields, after renaming (with slight abuse of notation)

$$C_d \to c,\ r_d \to r,\ t_d \to t \tag{56}$$

the equation (which is equation (21) from [13])

$$\frac{\partial c}{\partial t} + \frac{1}{r}\frac{\partial c}{\partial r} - \frac{1}{Pe}\frac{1}{r}\frac{\partial}{\partial r}\left(r\frac{\partial c}{\partial r}\right) = -Da_I c, \tag{57}$$

where we defined the Peclet number and the first Damkohler number

$$Pe = \frac{r_c^2 t_c}{D} = \frac{r_c v_c}{D},\ Da_I = \frac{SA\cdot K_{diss}t_c}{C_0} = \frac{SA\cdot K_{diss}r_c}{C_0 v_c}. \tag{58}$$

Sometimes the second Damkohler number is used, defined as follows

$$Da_{II} = \frac{SA\cdot K_{diss}r_c^2}{C_0 D} = PeDa_I. \tag{59}$$

Finally the dimensionless injection boundary condition (36) is given as

$$c(\tilde{r}_w, t) = c^\star + \frac{1}{Pe}\cdot\tilde{r}_w\frac{\partial c}{\partial r}(\tilde{r}_w, t), \tag{60}$$

where we defined the dimensionless injection well radius and the the dimensionless injection concentration as

$$\tilde{r}_w = \frac{r_w}{r_c},\ c^\star = \frac{C^{inj} - C_0}{C_0}. \tag{61}$$

Far away the boundary condition (38) reads

$$\frac{\partial c}{\partial r} \to 0 \text{ as } r \to \infty, \tag{62}$$

with slight abuse of notation, as the r in equation (38) refers to the dimensionless radial variable.

3.4 Analytical solutions

Due to our simplifying assumptions, equation (57) is now linear, which means that we can write the solution as the sum of a steady state (which will eventually be reached) and transients, i.e.,

$$c(r, t) = c_{ss}(r) + c_{tr}(r, t), \tag{63}$$

where $c_{ss}(r)$ satisfies the ODE

$$\frac{1}{r}\frac{dc_{ss}}{dr} - \frac{1}{Pe}\frac{1}{r}\frac{d}{dr}\left(r\frac{dc_{ss}}{dr}\right) = -Da_I c_{ss}, \tag{64}$$

with boundary conditions

$$c_{ss}(\tilde{r}_w, t) = c^\star + \frac{1}{Pe}\cdot\tilde{r}_w\frac{dc_{ss}}{dr}(\tilde{r}_w, t),\ \frac{dc_{ss}}{dr} \to 0 \text{ as } r \to \infty. \tag{65}$$

The solutions for different ranges of (Da_I, Pe)-values are

Regime A: $Da_I \ll Pe$ Diffusion can be neglected and we find

$$c_{ss}(r) = c^\star e^{-\frac{Da_I}{2}(r^2-\tilde{r}_w^2)},$$

provided $Pe \gg 1$.

Regime B: $Da_I \sim Pe$ All terms taken into account, $\beta = \frac{Da_I}{Pe}$ is order one. We find

$$c_{ss}(r) = \frac{c^\star}{1+\frac{1}{2}(\sqrt{1+4\beta}-1)}e^{-\frac{Pe}{2}(\sqrt{1+4\beta}-1)(r-\tilde{r}_w)}$$

Regime C: $Da_I \gg Pe$ Convection can be neglected and we find

$$c_{ss}(r) = c^\star\sqrt{\frac{Pe}{Da_I}}e^{-\sqrt{PeDa_I}(r-\tilde{r}_w)}.$$

4 Numerical approach (task 2b)

4.1 How to model mineral precipitation in a reservoir using PHREEQC, COMSOL and iCP

A general description of how to set up such a model is described by the software provider *iMaGe Modelling* in their user manual for interface COMSOL-PHREEQC (iCP). We based our model on example 2, provided by iMaGe Modelling. See Figure 1 for an overview of the communication between COMSOL, iCP and PHREEQC; [14] provides an elaborate description of the COMSOL-PHREEQC interface.

Here we only provide comments on how our model is set up and what our considerations were.

4.1.1 Setting up PHREEQC

Boundary and domain input files and database Three PHREEQC input files need to be prepared, the boundary and domain input files and the database.

BoundaryWater The boundary file describes the water that is injected into the reservoir. What to take into account:

- Temperature: equal to the injected water temperature.
- Pressure: equal to that in process facility downstream of heat exchanger; pressure impacts amount of gas dissolved in water and thereby pH.
- pH: take into account that CO_2 may be dissolved in the process water, which comes out of solution before it is analyzed in the lab, therefore account for it by using the EQUILIBRIUM_PHASES keyword data block. Set pH in water equal to the value measured in lab.
- Elements: preference for water samples that were taken as downstream as possible; filtration may impact the water composition, thus the composition of unfiltered samples may give a misleading view of the injected water. When using a comprehensive water analysis, include all elements, even the ones below 50 ppm in concentration.

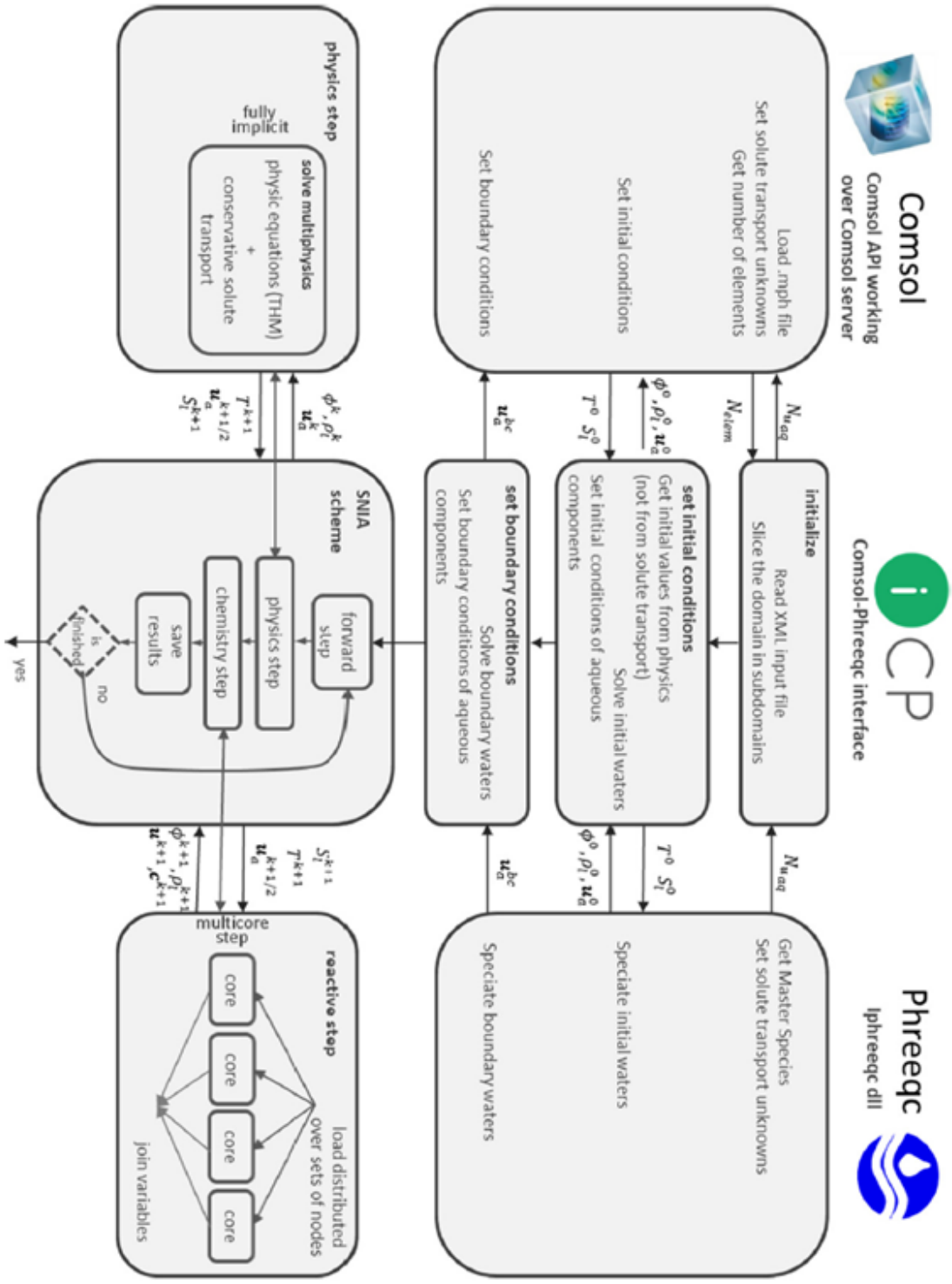

Figure 1: Communication between COMSOL, iCP and PHREEQC, from [14].

- EQUILIBRIUM_PHASES: CO_2, and CH_4 may be dissolved in the process water and may be assumed to be at equilibrium downstream of the degasser. Check with the process engineer what type of degasser is used, which may impact the amount of dissolved gas. CO_2 will impact the pH and solubility of the dissolved minerals, whereas CH_4 may impact the redox potential of the water (which is not included in our model of field case A).

ChemicalDomain The domain input file describes the near well-bore area. Here we assume that at time=0s the water composition is at equilibrium and has the same temperature as the injected water temperature; this ensures that we only model precipitation reactions from the processed water due to changes that occurred within processing facility.

- Temperature: here we assume it is equal to the injected water temperature; we are interested in the near wellbore area and assume this area has reached the injection water temperature almost instantaneously on the time span of geothermal field exploitation.
- Pressure: equal to that in process facility downstream of heat degasser; pressure impacts amount of gas dissolved in water and thereby pH. Although the pressure in the reservoir is higher in the reservoir than in the process facility, we assume no additional gas dissolves into the water downstream of the degasser and can therefore be assumed to be equal to the pressure at the heat-exchanger.
- pH: take into account that CO_2 may be dissolved in the process water, which comes out of solution before it is analyzed in the lab, therefore account for it by using the EQUILIBRIUM_PHASES keyword data block. Set pH equal to the value measured in lab.
- Elements: composition is based on the same water analyses as used for the BoundaryWater. However, we assume that this water has already reached equilibrium, and set the concentrations of various elements such that the saturation index (SI) of these minerals becomes equal to 0.
- EQUILIBRIUM_PHASES: CO_2 may be dissolved in the process water and may be assumed to be at equilibrium downstream of the degasser. Check with the process engineer what type of degasser is used, which may impact the amount of dissolved gas.
- PITZER: here we do not use specific-ion-interaction parameters for the Pitzer aqueous model because this significantly slows down the numerical simulation.

Database In this report the database is compiled from different sources, mainly: the lawrence livermore national laboratory (llnl) database in PHREEQC, [5, 6, 15]. Data on kinetics of dissolution and precipitation of minerals is not as widely available as data on solubility constants. The database used for this study is available under section 7.1. When deciding which source to use for the database, consider the experimental conditions under which the experiments were conducted.

4.1.2 Setting up COMSOL

Example 2 of iCP or this case study can be tailored for your own case. The following items in COMSOL need to be considered.

Parameters Define parameters and their values here, including them under parameters will allow for easy modification in calculations.

Geometry Here we modeled the geometry accounting for the well radius and the domain of interest. We use a *1D asymmetric* geometry in COMSOL, with which we model radial flow in the near well bore area and radial symmetry. See Figure 2 for a schematic of the reservoir that we are effectively modeling.

Darcy's Law Here we define the input parameters for the Darcy flow equation, which were also defined under *parameters*. We assume a fixed pressure at the outlet, equal to the initial pressure; at the inlet we assume a fixed inflow velocity.

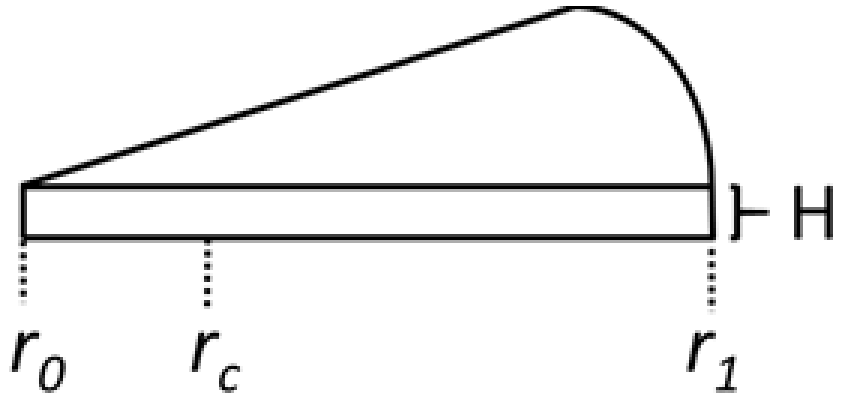

Figure 2: Schematic of our reservoir model. Here r_c, the characteristic length, equal to well radius, r_1 is equal to the full domain we are interested in. In our case H is equal to 1m.

Molal Solute Transport Here we define the input parameters for the transport of ions in the water: advection, which is defined as darcy flow, and diffusion, which is defined as the porosity$\times 10^{-8}$ [m^2/s]. Here we assume a

Mesh For the mesh we define a mesh which is finer near the inlet than near the outlet; with 100 elements, element growth rate of 1.3 and a maximum element size of 0.001m.

Study Under study we define the order of the different calculations; here under step 1 first the darcy and molal solute transport equations are solved, followed by step 2, importing the results from phreeqc.

4.1.3 Setting up iCP

Timestepping The stepsizes can be included under $\ll iCP \setminus timeStepList \setminus timeStep1 \gg$. Under *endTime* you can define the total simulation time and under *numOfIntervals* the number of intervals, which is used to calcualte the timestep (endTime-initialTime)/numOfIntervals.

Minerals and ions Minerals and ions can be included under $\ll phreeqcRocks \setminus selectedOutputList \setminus output1 \gg$. Include the relevant ions and minerals under *activities*, ions under *molalities*, and minerals under *saturation_indeces*, *kinetic_reactants* and *kinetic_reactants_delta*. To check the simulation output, also include under *general* pH, pe, temperature, ionic_strength and charge. If desired, the change in mineral volume (and thereby the porosity) can be calculated by include under *punch* a code similar to the script below; in PHREEQC define the number of moles of the different minerals at time = 0s. See example 2 provided by iMaGe with the iCP software package.

```
"punch" : [{
"name" : "mineralVolume",
"definition" :
"KIN('Fluorite')*2.454e-5+KIN('Quartz')*2.269e-5"
}, {
"name" : "waterMassFraction",
"definition" : "TOT('water')/(RHO*SOLN_VOL)"
}
]
```

4.2 Validation of the numerical model with the analytic model of section 3

Here we validate our numerical model with the analytical model described in section 3 and in [13]. We inject water, supersaturated with the mineral celestite, strontium sulphate ($SrSO_4$), into a porous medium. The concentration of dissolved strontium is calculated over a distance of 100 times the characteristic distance, which is equal to the well radius. Relevant properties of the water, porous

medium and the reaction kinetics are given in tables 6, 2 and 1. Here the precipitation of Celestite does not impact the acidity of the water and the reaction kinetics are not a function of the pH. Figure 3 shows that the numerical and analytical result are practically identical, and thereby serves as a verification of our analytical model.

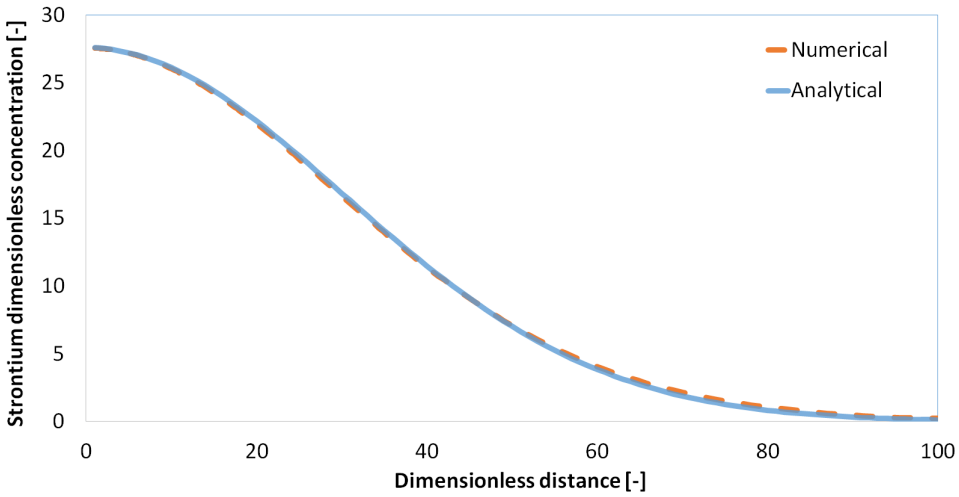

Figure 3: Dimensionless strontium concentration in water against dimensionless distance from injection well for water, super-saturated with Celestite, injected into a reservoir. Input parameters are given in table 1.

Equilibrium constants	
A1	3.55E+03
A2	1.21E+00
A3	-1.33E+05
A4	-1.41E+03
A5	5.08E+06
A6	-4.55E-04
Kinetic parameters	
A, Arrhenius pre-exponential factor [m^{-2} s^{-1}]	4.65E-02
E_a Activation energy [J mol^{-1}]	34000
η [-]	2
θ [-]	0.5
Injection water composition [mol/kgw]	
Na^+	1.84×10^{-1}
Cl^-	4×10^{-3}
Sr^{2+}	10^{-2}
$SO_4{}^{2-}$	10^{-1}
Reservoir water composition [mol/kgw]	
Na^+	2.033×10^{-1}
Cl^-	4×10^{-3}
Sr^{2+}	3.5×10^{-4}
$SO_4{}^{2-}$	10^{-1}

Table 1: Celestite kinetics parameters and equilibrium constant.

4.3 Uncertainty of kinetic parameters and the uncertainty range of the numerical results (task 1b)

We find that to make meaningful predictions on mineral precipitation in the near wellbore region, the activation energy should be known within a margin of error smaller than 15%, the pre-exponential

Reservoir properties and injection rate	
Porosity [-]	0.15
Reservoir thickness [m]	30
Injection rate [m^3hr^{-1}]	300
Reservoir temperature [°C]	80
Injection water temperature [°C]	80
Well radius [m]	0.05
Region of interest [m]	1
Diffusion coefficient [m^2s^{-1}]	1.5×10^{-9}

Table 2: Relevant properties of the modelled reservoir and injection flux.

constant within a margin of error equal to or smaller than one order of magnitude, and the reactive surface area within a range smaller than two orders of magnitude. We suggest to conduct relevant laboratory experiments to determine the kinetic reaction speed, $SA\times A\times e^{-\frac{E_a}{R\times 308[K]}}$ to increase confidence in modelling mineralization in a specific geothermal field. For the purpose of modelling mineralization in geothermal facility and field, it may not be necessary to determine the individual parameters and the product of the parameters may suffice if the injection temperature is fixed at 35°C. These experiments should focus on the mineralization reaction with 'intermediate' kinetics.

To illustrate the uncertainty in kinetic reaction modelling, in this section we model quartz precipitation near the injection well bore area, using the minimum and maximum input parameters reported in [5, 15], see Tables 3 and 4. Here we assume the uncertainty range in the equilibrium constant is negligible.

We use the analytic model described in section 3.4 to obtain the steady-state solutions to illustrate the uncertainty range in mineralization modelling.

See Figure 4 for the steady-state solution range of dissolved quartz concentrations near the injection well and Table 5 for the dimensionless quartz concentration at a dimensionless distance of 100.

Table 5 shows amount of supersaturated quartz that may precipitate in our case is the range of 1% and 99%, and the reaction rate can differ by 7 orders of magnitude, depending on the chosen input parameters. This uncertainty range is wider than observed by [12] in their systematic review of forsterite dissolution rate data, where they observe ± 300% relative error in the reaction rate.

4.3.1 Activation energy

It shows that the level of activation energy is a deciding factor whether less than 1% of quartz will precipitate or more than 99% in our region of interest. The four solutions with the lowest values all have the lowest activation energy. In our case the activation energy factor is between 68 and 90 [kJ $mole^{-1}$], i.e. 79 ± 15%. We therefore conclude that the activation energy should be known within a margin of error smaller than 15% to make meaningful predictions on mineral precipitation in the near wellbore region.

4.3.2 Reactive surface area

Within the subset of input parameters with minimum activation energy, the reactive surface area value uncertainty leads to an uncertainty range in mineralization of 96%. Whereas within the subset of input parameters with maximum activation energy, the reactive surface area value uncertainty leads to a mineralization uncertainty range of 1%. We judge this range of uncertainty as unacceptable within the context of this work. In our case the reactive surface area has a value between 200 and 20000 [m^2kg^{-1}]. We therefore conclude that the reactive surface area should be known within a range smaller than two orders of magnitude to make meaningful predictions on mineral precipitation in the near wellbore region.

4.3.3 Pre-exponential constant

Within the subset of input parameters with minimum activation energy, the pre-exponential constant uncertainty leads to an uncertainty range in mineralization of 2%. Whereas within the subset of input

parameters with maximum activation energy, the reactive surface area value uncertainty leads to a mineralization uncertainty range of 38%. We judge this range of uncertainty as acceptable within the context of this work. In our case the pre-exponential factor has a value between 23.3 and 333. We therefore conclude that the pre-exponential factor should be known within a range of an order of magnitude to make meaningful predictions on mineral precipitation in the near wellbore region.

4.3.4 Methodologies to determine the reactive surface area of a mineral and which methodology is more relevant for field case modelling

We suggest to use a geometric surface area when modelling mineral precipitation, and give our reasoning here.
Surface area per weight unit of mineral is usually measured using a Brunauer–Emmett–Teller (BET) methodology [16] or geometric surface area [17]. With the BET methodology the surface area is determined by first separating individual mineral grains and determining their surface area by a gas adsorption experiment, whereas with the geometric methodology the surface area is estimated based on the grain size and surface roughness. [12] conducted a systematic literature review of forsterite dissolution rate data and find that rates based on geometric surface area are faster than those based on BET surfaces by a factor 5. [18] find that assuming that all the mineral surfaces are available for mineralization, as is done with the BET methodology, results in an over-estimation of their observed reaction rates by a factor 10-20. [17] find that using image-based specific surface area values, i.e. a form of geometric surface area, resulted in their best match between their modelling and laboratory experimental results.
[12] note that there are three reasons that geometric surface area based rates are preferred over BET surface area based rates for modelling field cases: reliability of the results, cost and ease of procedure.

Kinetic reaction parameters		
Arrhenius equation parameters	minimum	maximum
Pre-exponential factor, A [mole m^{-2} s^{-1}]	23.3	333
Activation energy E_a [kJ $mole^{-1}$]	68	90
Reactive surface area [m^2kg^{-1}]	200	20000
Equilibrium constants		
a1	0.077698	
a2	0.010612	
a3	3465.1	
a4	-4.3551	
a5	-721380	

Table 3: Kinetic reaction parameters with their assumed uncertainty ranges, from [15] and [5].

Relevant field parameters	
Porosity [-]	0.15
Reservoir thickness [m]	30
Injection rate [m^3hr^{-1}]	300
Well radius [m]	0.05
Diffusion [m^2s^{-1}]	1.5×10^{-9}
Temperature (reservoir and injection water) [°C]	35
SiO_2 injection concentration [mol kgw^{-1}]	5.45×10^{-4}
SiO_2 steady-state concentration [mol kgw^{-1}]	1.58×10^{-4}

Table 4: Relevant properties of the modelled reservoir and injection flux.

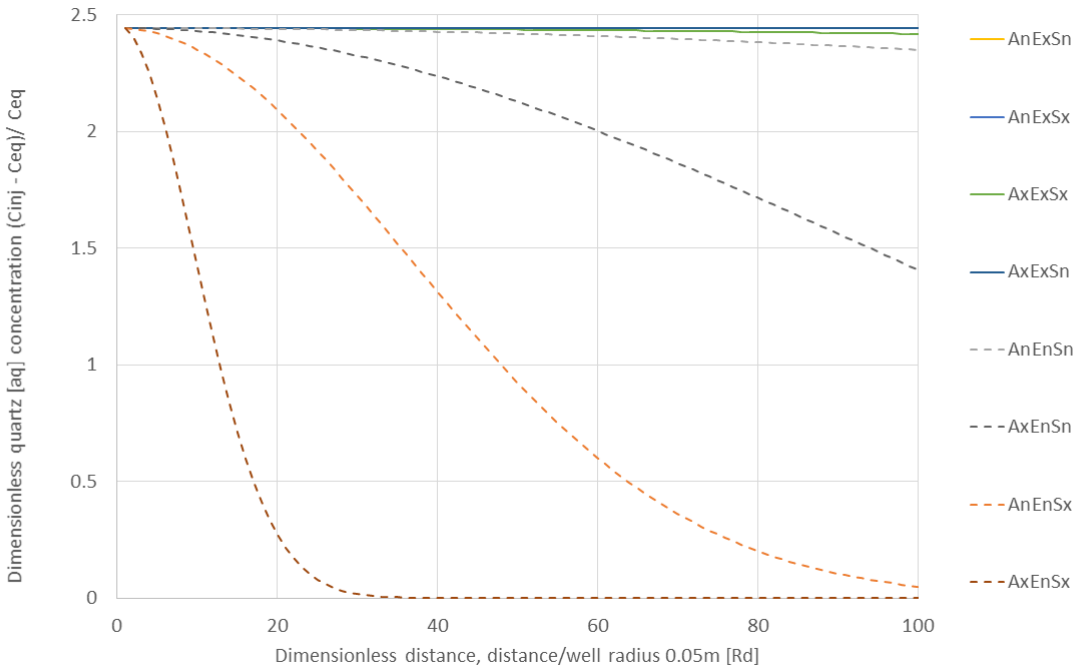

Figure 4: Uncertainty range of quartz [aq] dimensionless concentration as a function of dimensionless distance from the injection well. The abbreviations in the legend are as follows: A is the pre-exponential factor [mole m^{-2} s^{-1}], E is the activation energy [kJ $mole^{-1}$], S is the reactive surface area [m^2kg^{-1}], n is the minimum value, x is the maximum value

4.4 Numerical modelling of mineral precipitation in the near wellbore area of field case A

Here we model the mineral precipitation in the near wellbore area of field case A. First we model the water in process facility under the conditions at the well-head of the injection well, see table 7 for the water composition, table 8 for a list of the minerals with which the water is supersaturated and Table 9 for an injection well scale analysis. These analyses show that the minerals with an SI larger than 0 are not necessarily the minerals forming a scale in the injection well. This can be due to the database being based on experimental results that are not representative of our situation or that the minerals with an SI larger than 0 do not necessarily precipitate within the process facility. The minerals that have an SI larger than 0 and are also present in the injection well scale, are used model mineral precipitation in the near well-bore area, over period of one pore volume (400 seconds), see figures 5 and 6 and table 2. We find that the amount of moles of galena and quartz to precipitate in the near well-bore area are not in the same proportion to the amount of fluorite and chalcopyrite to precipitate as found in the injection well, see table 9. This indicates that that the amount of galena and quartz scale found in the injection well and likely in the near wellbore area are formed upstream, and possible produced in solid phase at the production well head.

Analytical model results			
Case variant	(C - C_{eq})× C_{eq}^{-1} [-]	C×C_{eq}^{-1} [%]	SA×A×$e^{-\frac{Ea}{R\times 308[K]}}$
AnExSn	2.44	100	2.59E-13
AxExSn	2.44	100	3.66E-12
AnExSx	2.44	100	2.59E-11
AxExSx	2.42	99	3.66E-10
AnEnSn	2.35	96	1.39E-09
AxEnSn	1.41	58	1.96E-08
AnEnSx	0.05	2	1.39E-07
AxEnSx	0.00	0	1.96E-06

Table 5: Steady-state analytical solutions with their dissolved quartz concentrations at a dimensionless distance of 100 from the injection well.

Water properties	
Temperature [°C]	80
pH [-]	7
pe [-]	4
Injection water composition [mol/kgw]	
Na^+	2.03×10^{-1}
Cl^-	4×10^{-3}
Sr^{2+}	3.5×10^{-4}
$SO_4{}^{2-}$	10^{-1}
Aquifer water composition [mol/kgw]	
Na^+	1.84×10^{-1}
Cl^-	4×10^{-3}
Sr^{2+}	10^{-2}
$SO_4{}^{2-}$	10^{-1}

Table 6: Water composition of the injection water and the aquifer water. Sodium is adjusted in PHREEQC to achieve ion charge balance.

Water composition field case A	
Anions, ppm	
Cl^-	85 000
Br^-	536
$SO_4{}^{2-}$	220
$HCO_3{}^-$	190
Cations, ppm	
Ba	8
Ca	6 100
Cu	0.1
F	18.1
Fe	67
K	275
Mg	1 000
Mn	1.3
Na	45 000
Pb	0.06
Si	20
Sr	400
Zn	0.2

Table 7: Water composition from field case A, averaged over the length of surface facility, measured using ICPMS and IC.

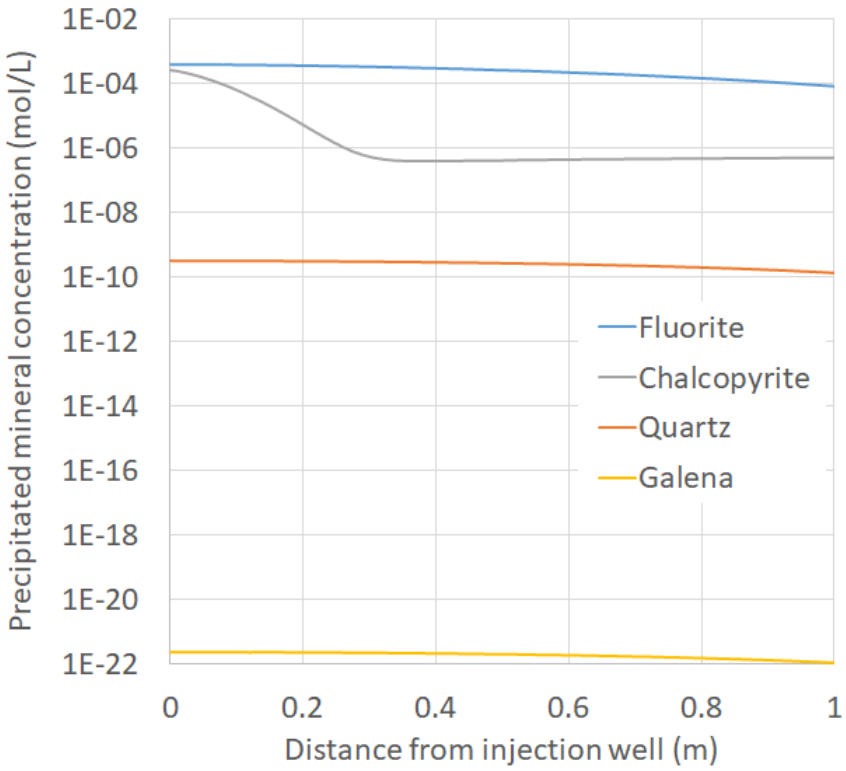

Figure 5: Precipitated mineral concentrations of fluorite, chalcopyrite, quartz, and galena the near well bore area of field case A.

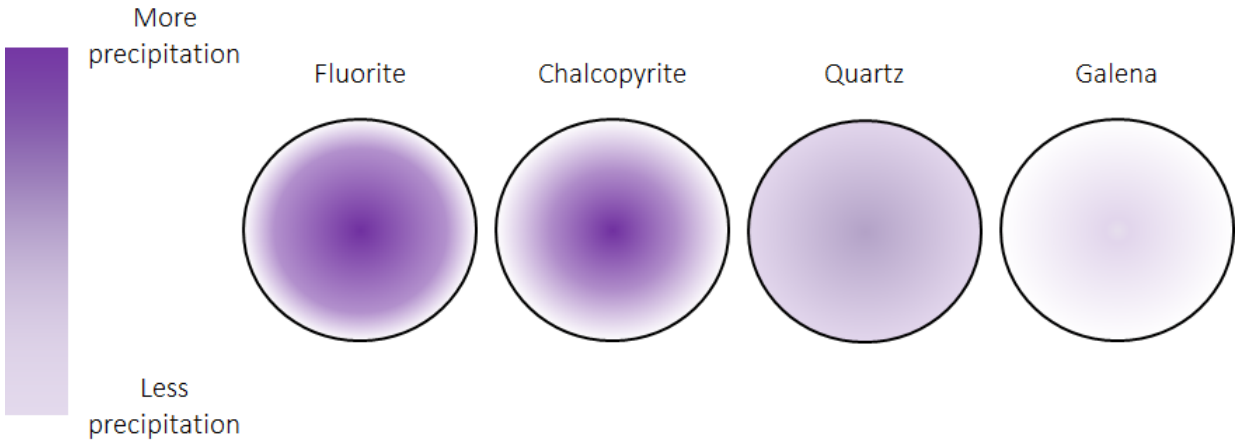

Figure 6: Schematic of precipitated mineral concentrations of fluorite, chalcopyrite, quartz, and galena the near well bore area (1 m radius) of field case A. Color indicates concentration, with dark purple indicating more mineral precipitation and light purple indicating less precipitation. Color is not to scale.

H

Minerals solubility indices		
Mineral	Chemical formula	Saturation index
Bornite	Cu_5FeS_4	21.38
Chalcopyrite	$CuFeS_2$	7.78
Chalcocite	Cu_2S	6.53
Pyrite	FeS_2	6.02
Covellite	CuS	3.78
Fluorite	CaF_2	1.65
Galena	PbS	3.06
Sellaite	MgF_2	2.69
Sphalerite	ZnS	1.67
Barite	$BaSO_4$	0.66
SrF_2	SrF_2	0.57
Quartz	SiO_2	0.36
Tridymite	SiO_2	0.18
Witherite	$BaCO_3$	0.12
Chalcedony	SiO_2	0.10

Table 8: Supersaturated minerals in produced water from case study A with their saturation indices and the minerals modelled in the reservoir case are highlighted in yellow. Part of WP1.

Scale composition of injection well		
Mineral	Chemical formula	Weight %
Quartz	SiO_2	25.3
Galena	PbS	15.1
Magnesioferrite	Fe_2MgO_4	8.8
Lepidocrocite	FeO(OH)	8.3
Lead	Pb	6.9
Fluorite	CaF_2	6.8
Goethite	FeO(OH)	6.8
Halite	NaCl	5.7
Chalcopyrite	$CuFeS_2$	4.4
Talc	$Mg_3(OH)_2(Si_4O_{10})$	3.5
Montetrisaite	$Cu_6(SO_4)(OH)_{10}.2H_2O$	2.9
Zinc	Zn	2.0
Muscovite	$KAl_3(OH)_2Si_4O_{10}$	1.9
Hematite	Fe_2O_3	1.7

Table 9: Scale composition retrieved from injection well, field case A, with the minerals modelled to precipitate in the reservoir highlighted in orange. Note the absence of barite. Part of WP1.

5 Decision tree (task 3b)

We composed two decision trees, based on data from: 1) filter residues, see Figures 7 and 2) PHREEQC modelling results, see Figure 8. The mentioned mitigation strategies are non-chemical based and we assume no redox reactions occurred.

5.1 Decision tree based on filter residues

The decision tree based on filter residues will require XRD/XRF analyses to determine the filter residue composition. Due to reaction kinetics, the starting point of the precipitation reaction may be difficult to induce. For particles with a radius larger than the filter mesh size, the filter beta is equal

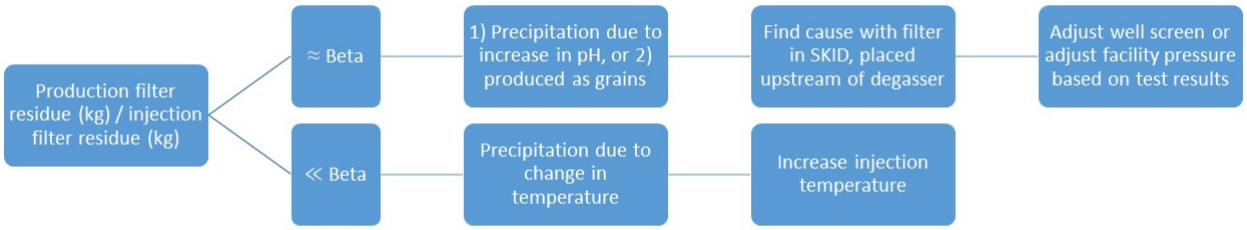

Figure 7: Using the efficiency of the filters and the mass of filter residues it can be deduced the likely location of where the precipitate has formed. Suggested mitigation strategies are non-chemical based.

to the ratio of the amount of solids upstream and downstream of the filter. The beta can be as high as 5000 in geothermal processing facilities. So in cases where there is a production filter and an injection filter with the same mesh size, the ratio of the amount of residues collected serve as an indication of where the precipitation reaction started and therefore its mitigation strategies, see Figure 7.
Similarly, in cases where there is an unacceptable amount of filter residue in the production filters, it can be distinguished if the solids where produced from the well head or if they formed after the heat exchanger by placing the SKID between the well-head and degasser. If the accumulation rate of the solids is similar between the well-head and degasser as in the production filter, then the solids were produced at the well-head.

5.2 Decision tree based on PHREEQC results

PHREEQC modelling will show the saturation indexes of the different minerals in the database; it is therefore important that the database is complete and the database is based on experiments conducted under similar conditions as in the process facility. The saturation index will indicate whether the water is supersaturated with a specific mineral, and thus if a precipitation reaction may initiate. Where in the process facility the SI is larger than 0 for the first time, can be used to understand due to what physical processes the water has become supersaturated with the mineral and thereby a possible mitigation strategy, see Figure 8.

6 Discussion

There is a discrepancy between the list of super saturated minerals from PHREEQC (see Table 8) and the scale composition of the injection well (see Table 9). The discrepancy can be due to a combination of various reasons, among others: A) incorrect water composition, B) incomplete or incorrect database in PHREEQC, C) scale composition includes minerals produced in solid form from the subsurface, D) incorrect scale composition of injection well, E) minerals forming by interactions with the metal in the process facility [19].

For further studies we suggest to create a local-equilibrium and kinetic database of relevant minerals by conducting experiments on the produced water under field and process conditions.

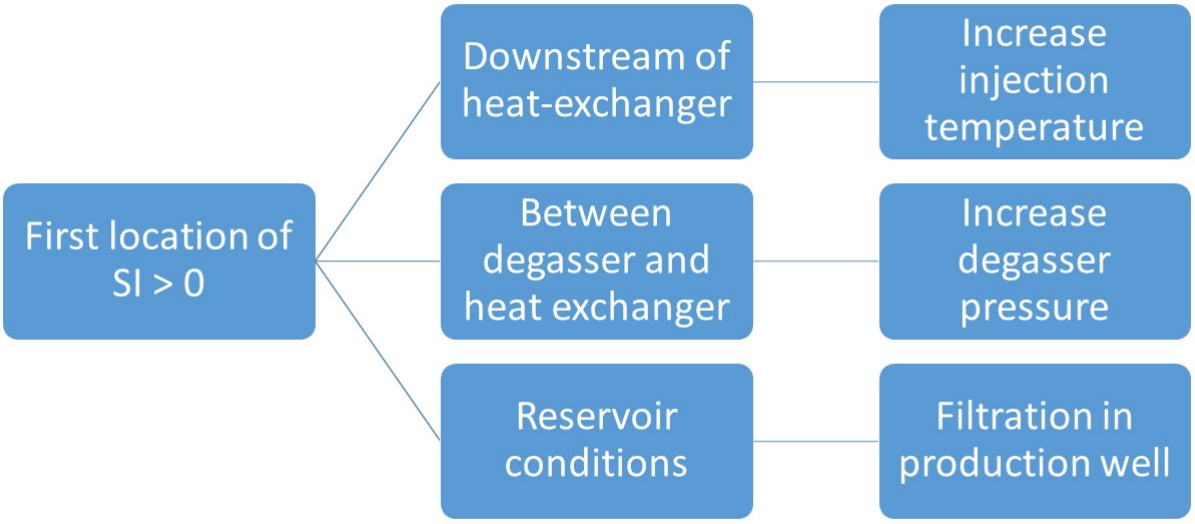

Figure 8: The solubility index (SI) indicates whether the solution is super-saturated with a specific mineral. Suggested mitigation strategies are non-chemical based.

References

[1] Antonio C Lasaga. *Kinetic theory in the earth sciences*. Princeton university press, 2014.

[2] Yujuan Su, Fengtian Yang, Bing Wang, Zhi Jia, and Zhongfeng Duan. Reinjection of cooled water into sandstone geothermal reservoirs in china: a review. *Geosciences Journal*, 22(1):199–207, 2018.

[3] Nicolas CM Marty, Virginie Hamm, Christelle Castillo, Dominique Thiéry, and Christophe Kervévan. Modelling water-rock interactions due to long-term cooled-brine reinjection in the dogger carbonate aquifer (paris basin) based on in-situ geothermal well data. *Geothermics*, 88:101899, 2020.

[4] Pierre Ungemach. Reinjection of cooled geothermal brines into sandstone reservoirs. *Geothermics*, 32(4-6):743–761, 2003.

[5] James L Palandri and Yousif K Kharaka. A compilation of rate parameters of water-mineral interaction kinetics for application to geochemical modeling. Technical report, Geological Survey Menlo Park CA, 2004.

[6] Nicolas CM Marty, Francis Claret, Arnault Lassin, Joachim Tremosa, Philippe Blanc, Benoit Madé, Eric Giffaut, Benoit Cochepin, and Christophe Tournassat. A database of dissolution and precipitation rates for clay-rocks minerals. *Applied Geochemistry*, 55:108–118, 2015.

[7] C Anthony J Appelo and Dieke Postma. *Geochemistry, groundwater and pollution*. CRC press, 2004.

[8] James G Brown and Pierre D Glynn. Kinetic dissolution of carbonates and mn oxides in acidic water: measurement of in situ field rates and reactive transport modeling. *Applied Geochemistry*, 18(8):1225–1239, 2003.

[9] Simona Regenspurg, Ives Geigenmüller, Harald Milsch, and Michael Kühn. Copper precipitation as consequence of steel corrosion in a flow-through experiment mimicking a geothermal production well. *Geothermal Energy*, 5(1):1–15, 2017.

[10] Ugo Schwertmann. Solubility and dissolution of iron oxides. *Plant and soil*, 130(1):1–25, 1991.

[11] Yilun Zhang, Bin Hu, Yanguo Teng, Kevin Tu, and Chen Zhu. A library of basic scripts of reaction rates for geochemical modeling using phreeqc. *Computers & Geosciences*, 133:104316, 2019.

[12] J Donald Rimstidt, Susan L Brantley, and Amanda A Olsen. Systematic review of forsterite dissolution rate data. *Geochimica et Cosmochimica Acta*, 99:159–178, 2012.

[13] Bernard Meulenbroek, Rouhi Farajzadeh, and Hans Bruining. Process-based upscaling of reactive flow in geological formations. *International Journal of Heat and Mass Transfer*, 157:119969, 2020.

[14] Albert Nardi, Andrés Idiart, Paolo Trinchero, Luis Manuel de Vries, and Jorge Molinero. Interface comsol-phreeqc (icp), an efficient numerical framework for the solution of coupled multiphysics and geochemistry. *Computers & Geosciences*, 69:10–21, 2014.

[15] Jay R Black, Susan A Carroll, and Ralf R Haese. Rates of mineral dissolution under co2 storage conditions. *Chemical Geology*, 399:134–144, 2015.

[16] Majid Naderi. Surface area: brunauer–emmett–teller (bet). In *Progress in filtration and separation*, pages 585–608. Elsevier, 2015.

[17] Lauren E Beckingham, Elizabeth H Mitnick, Carl I Steefel, Shuo Zhang, Marco Voltolini, Alexander M Swift, Li Yang, David R Cole, Julia M Sheets, Jonathan B Ajo-Franklin, et al. Evaluation of mineral reactive surface area estimates for prediction of reactivity of a multi-mineral sediment. *Geochimica et Cosmochimica Acta*, 188:310–329, 2016.

[18] Lauren E Beckingham, Carl I Steefel, Alexander M Swift, Marco Voltolini, Li Yang, Lawrence M Anovitz, Julia M Sheets, David R Cole, Timothy J Kneafsey, Elizabeth H Mitnick, et al. Evaluation of accessible mineral surface areas for improved prediction of mineral reaction rates in porous media. *Geochimica et Cosmochimica Acta*, 205:31–49, 2017.

[19] FA Hartog, G Jonkers, AP Schmidt, and RD Schuiling. Lead deposits in dutch natural gas systems. *SPE production & facilities*, 17(02):122–128, 2002.

[20] JM Delany and SR Lundeen. The llnl thermochemical data base–revised data and file format for the eq3/6 package. Technical report, Lawrence Livermore National Lab.(LLNL), Livermore, CA (United States), 1991.

[21] Patricia Acero, Jordi Cama, and Carlos Ayora. Sphalerite dissolution kinetics in acidic environment. *Applied Geochemistry*, 22(9):1872–1883, 2007.

[22] Oleg S Pokrovsky, Sergey V Golubev, and Jacques Schott. Dissolution kinetics of calcite, dolomite and magnesite at 25 c and 0 to 50 atm pco2. *Chemical geology*, 217(3-4):239–255, 2005.

[23] Niko Kampman, Mike Bickle, John Becker, Nelly Assayag, and Hazel Chapman. Feldspar dissolution kinetics and gibbs free energy dependence in a co2-enriched groundwater system, green river, utah. *Earth and Planetary Science Letters*, 284(3-4):473–488, 2009.

[24] Andrew G Christy and Andrew Putnis. The kinetics of barite dissolution and precipitation in water and sodium chloride brines at 44–85 c. *Geochimica et Cosmochimica Acta*, 57(10):2161–2168, 1993.

7 Appendices

7.1 Appendix A - numerical modelling of mineral precipitation in the near wellbore area

7.2 PHREEQC files

7.2.1 PHREEQC input file

boundaryWater

```
SOLUTION 1 Process water
  pressure 1
        pH      6
        density 1.0917
        temp    22.5
  units   mg/l

    Na        45000 charge
    #Al   0.0012 #ICPMS/IC
    Ba   8 #ICPMS/IC
    Br   536 #ICPMS/IC
    Cl        85000 #ICPMS/IC
    Ca        6100 #ICPMS, SGS 5900
    Cu   0.109 #Cu2+, ICPMS/IC
    F   181 #ICPMS/IC
    Fe   67 #Fe2+ ICPMS/IC
    K   275 #ICPMS, SGS 260
    Mg   1000 #ICPMS, SGS 850, IC 168
    Mn   1.3 #ICPMS/IC, SGS 1.5
    Pb   0.060 #ICPMS 3-43, SGS 0.060
    S(+6)   220 #SO4 2-, SGS 220, ICPMS 213
    Si    20 #SiO2, ICPMS laat waarde zien tussen 10 en 20 ppb Si
    Sr   400 #SGS
    Zn   0.2 #ICPMS tussen 0.1 en 0.75, SGS zware metalen 0.130
    Alkalinity 190 as HCO3 #SGS
    -water    1 # kg

#PITZER
# -macinnes true
# -use_etheta true
# -redox true

SAVE SOLUTION 1
END

#PHASES
#Galena
# PbS + 1.0000 H+ = 1.0000 HS- + 1.0000 Pb+2
# -analytic 1.909920e+003 6.546249e-001 -7.577074e+004 -7.575379e+002 2.733540e+006 -2.484938e
# -Vm  31.4900
#-steps 1 day 24 steps


#Fix_H+
#H+ = H+
#log_K 0

GAS_PHASE 1 Gas phase
temperature 0 C
pressure 1 bar
volume 1.3909406 L
N2(g)       0.06395
CO2(g) 0.08574
CH4(g) 0.85030
```

```
SAVE GAS_PHASE 1
END

USE SOLUTION 1

REACTION_TEMPERATURE 1
35
REACTION_PRESSURE 1
9.2
USE GAS_PHASE 1

EQUILIBRIUM_PHASES
CH4(g) 0.0
CO2(g) 0.0 #dit stond er eerst niet in, bespreek met najoua

SAVE SOLUTION 2
END
```

chemicalDomain

```
SOLUTION 1 Process water
  pressure 1
        pH      6
        density 1.0917
        temp    22.5
  units   mg/l

    Na        45000 charge
    #Al   0.0012 #ICPMS/IC
    Ba   8 #ICPMS/IC
    Br   536 #ICPMS/IC
    Cl        85000 #ICPMS/IC
    Ca        6100 #ICPMS, SGS 5900
    Cu   0.109 #Cu2+, ICPMS/IC
    F   4 #181 #ICPMS/IC
    Fe   67 #Fe2+ ICPMS/IC
    K   275 #ICPMS, SGS 260
    Mg   1000 #ICPMS, SGS 850, IC 168
    Mn   1.3 #ICPMS/IC, SGS 1.5
    Pb   0.060 #ICPMS 3-43, SGS 0.060
    S(+6)   0.1 #220 #SO4 2-, SGS 220, ICPMS 213
    Si    5 #20 #SiO2, ICPMS laat waarde zien tussen 10 en 20 ppb Si
    Sr   400 #SGS
    Zn   0.2 #ICPMS tussen 0.1 en 0.75, SGS zware metalen 0.130
    Alkalinity 190 as HCO3 #SGS
    -water    1 # kg

SAVE SOLUTION 1
END

GAS_PHASE 1 Gas phase
temperature 0 C
pressure 1 bar
volume 1.3909406 L
N2(g)       0.06395
CO2(g) 0.08574
```

```
CH4(g) 0.85030


SAVE GAS_PHASE 1
END

USE SOLUTION 1

REACTION_TEMPERATURE 1
35
REACTION_PRESSURE 1
9.2
USE GAS_PHASE 1

EQUILIBRIUM_PHASES
CH4(g) 0.0
CO2(g) 0.0 #dit stond er eerst niet in, bespreek met najoua

SAVE SOLUTION 2
END

KINETICS 1
#-cvode true
#-cvode_steps 5000
#-cvode_order 5
-step_divide 4
-runge_kutta 3
-bad_step_max 500

Fluorite
       -m0 0
       -parms 1 1

Galena
       -m0 0
       -parms 1 1

Chalcopyrite
       -m0 0
       -parms 1 1

Quartz
       -m0 0
       -parms 1 1
```

7.2.2 PHREEQC database kinetics additions

Barite

```
############
#barite
############
barite
# from Palandri and Kharaka 2004
# experimental condition range T=40-90C, pH=2-6

-start
```

```
1 rem unit should be mol,kgw-1 and second-1
2 rem parm(1) is surface area in the unit of m2/kgw
3 rem calculation of surface area can be found in the note
4 rem M is current moles of minerals. M0 is the initial moles of minerals
5 rem parm(2) is a correction factor
10 rem acid solution parameters
11 a1=3.09E-02
12 E1=30780
13 n1=0.220
20 rem neutral solution parameters
21 a2=3.13E-03
22 E2=30780
30 rem base solution parameters
31 a3=0
32 E3=0
33 n2=0
36 rem rate=0 if no minerals and undersaturated
40 SR_mineral=SR("barite")
41 if (M<0) then goto 200
42 if (M=0 and SR_mineral<1) then goto 200
43 if (M0<=0) then SA=PARM(1) else SA=PARM(1)*(M/M0)^0.67
50 if (SA<=0) then SA=1
60 R=8.31451
75 Rate1=a1*EXP(-E1/R/TK)*ACT("H+")^n1  #acid rate expression
80 Rate2=a2*EXP(-E2/R/TK)               #neutral rate expression
85 Rate3=a3*EXP(-E3/R/TK)*ACT("H+")^n2    #base rate expression
90 Rate=(Rate1+Rate2+Rate3)*(1-Sr_mineral)*SA*parm(2)
100 moles= rate*Time
200 save moles
-end
```

Fluorite

```
############
#Fluorite
############
Fluorite
# from Palandri and Kharaka 2004
# experimental condition range cannot be found

-start
1 rem unit should be mol,kgw-1 and second-1
2 rem parm(1) is surface area in the unit of m2/kgw
3 rem calculation of surface area can be found in the note
4 rem M is current moles of minerals. M0 is the initial moles of minerals
5 rem parm(2) is a correction factor
10 rem acid solution parameters
11 a1=4.46E+05
12 E1=73000
13 n1=1
20 rem neutral solution parameters
21 a2=9.99E-02
22 E2=73000
30 rem base solution parameters
31 a3=4.33E+02
32 E3=45700
```

```
33 n2=0.5
36 rem rate=0 if no minerals and undersaturated
40 SR_mineral=SR("Fluorite")
41 if (M<0) then goto 200
42 if (M=0 and SR_mineral<1) then goto 200
43 if (M0<=0) then SA=PARM(1) else SA=PARM(1)*(M/M0)^0.67
50 if (SA<=0) then SA=1
60 R=8.31451
75 Rate1=a1*EXP(-E1/R/TK)*ACT("H+")^n1  #acid rate expression
80 Rate2=a2*EXP(-E2/R/TK)               #neutral rate expression
85 Rate3=a3*EXP(-E3/R/TK)*ACT("H+")^n2    #base rate expression
90 Rate=(Rate1+Rate2+Rate3)*(1-Sr_mineral)*SA*parm(2)
100 moles= rate*Time
200 save moles
-end
```

Galena

```
################
# Galena (Acero et al, 2007)
################
Galena

# experimental condition range T=25-70C, pH=1-3

-start
1 rem unit should be mol,kgw-1 and second-1
2 rem parm(1) is surface area in the unit of m2/kgw
3 rem calculation of surface area can be found in the note
4 rem M is current moles of minerals
5 rem M0 is the initial moles of minerals
6 rem parm(2) is a correction factor
40 SR_mineral=SR("Galena")
41 if (M<0) then goto 200
42 if (M=0 and SR_mineral<1) then goto 200
43 if (M0<=0) then SA=PARM(1) else SA=PARM(1)*(M/M0)^0.67
50 if (SA<=0) then SA=1
60 R=8.31451
70 if (-LA("H+")<2) then J=10^-5.7*exp(-23000/R/TK)*ACT("H+")^0.43 else J=10^-8.5*exp(-15000/R
90 Rate=J*(1-Sr_mineral)*SA*parm(2)
100 moles=Rate*Time
200 save moles
-end
```

Quartz

```
###########
#Quartz Marty et al 2015
###########
quartz

# from Marty et al 2015
# pre-exponent coefficient A is calculated from logk using equation A=k/exp(-Ea/RT)
# experimental condition range T=25-300C, pH=2-13

-start
```

```
1 rem unit should be mol,kgw-1 and second-1
2 rem parm(1) is surface area in the unit of m2/kgw
3 rem calculation of surface area can be found in the note
4 rem M is current moles of minerals. M0 is the initial moles of minerals
5 rem parm(2) is a correction factor
10 rem acid solution parameters
11 a1=0
12 E1=0
13 n1=0
20 rem neutral solution parameters
21 a2=1.98
22 E2=77000
30 rem base solution parameters
31 a3=1.97E+04
32 E3=80000
33 n2=0.34
36 rem rate=0 if no minerals and undersaturated
40 SR_mineral=SR("quartz")
41 if (M<0) then goto 200
42 if (M=0 and SR_mineral<1) then goto 200
43 if (M0<=0) then SA=PARM(1) else SA=PARM(1)*(M/M0)^0.67
50 if (SA<=0) then SA=1
60 R=8.31451
75 Rate1=a1*EXP(-E1/R/TK)*ACT("H+")^n1  #acid rate expression
80 Rate2=a2*EXP(-E2/R/TK)               #neutral rate expression
85 Rate3=a3*EXP(-E3/R/TK)*ACT("OH-")^n2    #base rate expression
90 Rate=(Rate1+Rate2+Rate3)*(1-Sr_mineral)*SA*parm(2)
100 moles= rate*Time
200 save moles
-end
```

7.3 Appendix B - mineral precipitation in the geothermal process facility, approach used for task 3b

We investigate a field-case study where galena precipitate is filtered in a geothermal surface facility. We model this geothermal system in PHREEQC. The PHREEQC model shows that a significant fraction (approx. 85 wt.%) of the collected galena is produced in solid phase from the reservoir, and a smaller fraction (approx. 15 wt.%) is formed within the geothermal facility. We conduct a geological history and literature study, and we find that the radioactive Pb may originate from the Zechstein and Rotliegend, where it may have attached to the Copper shale formations. This study is described in detail in the attached report, titled '*A case-study of Pb-scaling in a geothermal project in the West Netherlands Basin*'.

7.4 Appendix C - databases (task 1a)

Databases for mineralisation, kinetic approach parameters and equilibrium constants. These data are collected from [5,6], and [15]. Not all data were collected within conditions of low-enthalpy geothermal projects in The Netherlands (pH: 4-7 and T: 35 - 90°C), nor were the kinetic approach parameters available for all relevant minerals, such as lepidocrocite and magnesioferrite.

Databases used:

- A compilation of rate parameters of water-mineral interaction kinetics for application to geochemical modeling [5].
- A library of BASIC scripts of reaction rates for geochemical modeling using PHREEQC [11].
- The LLNL thermochemical data base [20].

- Sphalerite dissolution kinetics in acidic environment [21].
- Dissolution kinetics of calcite, dolomite and magnesite at 25 °C and 0 to 50 atm pCO2 [22].
- Feldspar dissolution kinetics and Gibbs free energy dependence in a CO2-enriched groundwater system, Green River, Utah [23].
- Rates of mineral dissolution under CO2 storage conditions [15].
- The kinetics of barite dissolution and precipitation in water and sodium chloride brines at 44–85°C [24].
- Kinetic dissolution of carbonates and Mn oxides in acidic water: measurement of in situ field rates and reactive transport modeling [8].

7.5 Description of field case (part of task 3a)

The field case we use for our modelling purposes is a low-enthalpy geothermal project located in the West Netherlands Basin. To reduce the likelihood of redox reactions occurring mainly glass fibre reinforced piping material is used and the heat exchanger is composed of a noble metal, but, in some parts of the facility water comes in contact with steel. Furthermore, no corrosion inhibitors or other chemicals are added to the water. This set up allows us mineral precipitation in a geothermal facility relatively undisturbed by redox reactions. We collected and analysed water samples at different points in the process facility (upstream of degasser; between degasser and production filters; between heat exchanger and injection filters; between injection filters and injection well) to investigate for trends in ion concentrations over the length of the process facility, but found none. See supplemental data-package for water composition.

7.5.1 collection and preparation of samples

Ten water samples were collected at a low-enthalpy geothermal heat-power plant, location 'A'. Two samples were collected at every sample-point. See figure 9 for a schematic of the power plant and the locations of the five sample-points. Samples collected at location A were from one production well, whereas the other samples came from a flow-stream that consisted of two water coming from two production wells. The samples were collected in 1-litre PP bottles; silica based bottles were avoided due to the possibility of it impacting the silicon concentrations. The samples were stored at room temperature for 24 hours and 48 hours, after which the samples were prepared for ion-chromatography (IC) and induced coupled plasma mass-spectrometer (ICP-MS) respectively. The analyzed samples were diluted ten times with milliQ water and nitric acid, with the final solution having a nitric acid concentration of 0.68 wt% HNO3. In the case of the IC analyses the solutions were immediately filtered (0.45 μm mesh, Chromafil Xtra) and in the case of ICP-MS the solutions were filtered 72 hours after dilution (0.20 μm mesh, Chromafil Xtra). The solutions were then diluted further, to achieve ion concentrations in the solutions within the measurement range of the IC and ICP-MS devices.

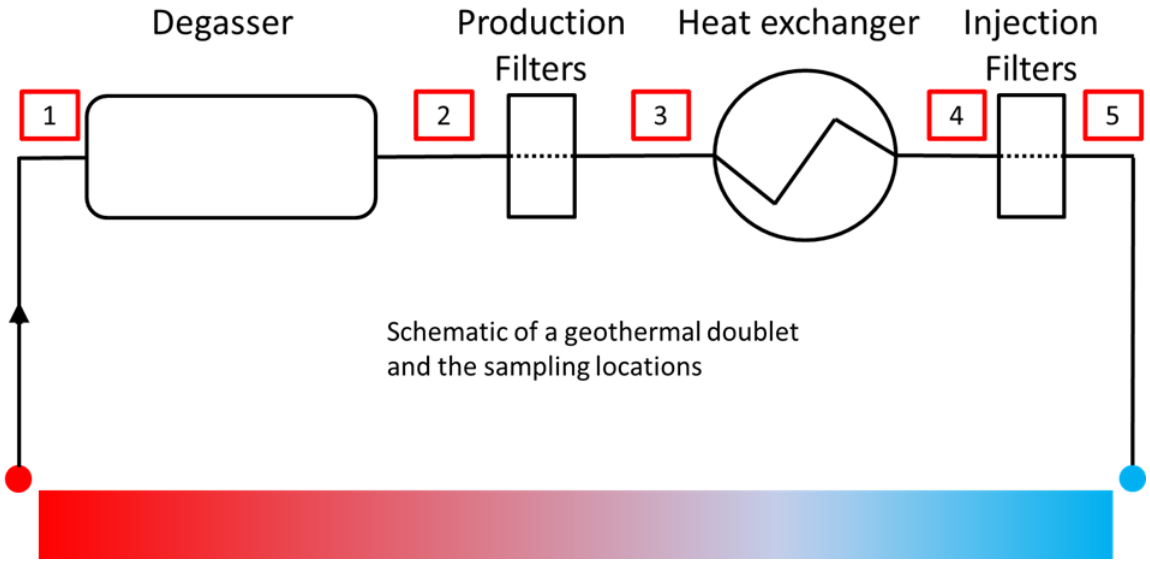

Figure 9: Schematic overview of a geothermal doublet and our sampling locations at field case A labelled numerically.